Equatorial rain forest lateritic mantles: A geomembrane filter

Fabrice Colin   Institut Français de Recherche Scientifique pour le Développement et la Coopération (ORSTOM) and
                  Laboratoire de Géosciences de L'Environnement, URA CNRS 132, Université Aix-Marseille III
                  13397 Marseille cédex 13, France

George H. Brimhall   Department of Geology and Geophysics, University of California, Berkeley, California 94720

Daniel Nahon   Laboratoire de Géosciences de l'Environnement, URA CNRS 132, Université Aix-Marseille III
                 13397 Marseille cédex 13, France

Christopher J. Lewis   Department of Geology and Geophysics, University of California, Berkeley, California 94720

Alain Baronnet   Centre de Recherche sur les Mécanismes de la Croissance Cristalline (CRMC2), CNRS
                   Université Aix-Marseille III, 13397 Marseille cédex 13, France

Kathy Danti   Department of Geology and Geophysics, University of California, Berkeley, California 94720

ABSTRACT

The superimposed weathering layers in equatorial rain forest lateritic mantles from Gabon, Africa, function as interactive compartments forming a dynamic semipermeable geomembrane filter. Selectivity of the filter is controlled by a progressive downward disappearance of connected macropore pathways created by bioturbation and dissolution. The natural balance of root activity, translocation, dissolution, deformation, and pore evolution leads to the development of porous and permeable, mature, open geochemical weathering systems at the expense of the lithosphere. These conclusions can be useful in modeling the fate of lateritic soils, which cover one-third of the emerged area of the world and which are economically important both as metal deposits and agricultural soils.

INTRODUCTION

Since Buchanan (1848, *in* Lacroix, 1914), the tropical weathering mantle (so-called "laterites") has been intensively but qualitatively studied from landscape scale to crystal scale (Millot, 1964; Nahon, 1991) to understand the genesis and evolution over geologic time of these surficial formations. Laterites are spread out over one-third of the emerged areas and are economically important both as metal deposits and as nutrient-

limited, but more and more utilized, agricultural soils (Sternberg, 1987; Lean and Warrilow, 1989; Anamosa et al., 1990).

In recent models for interactions of organisms with the subsurface rocks to produce soils, the soils are considered as a geomembrane interfacing the lithosphere with the biosphere, atmosphere, and hydrosphere (Arnold et al., 1990). We propose to extend this concept to entire weathering mantles and to begin quantifying the filtration role of the geomembrane by describing physical and chemical processes that lead to the formation of tropical weathering profiles. The method used in this work can be applied in studying most of the supergene weathering systems.

Our investigations have been conducted in the anthropogenically undisturbed equatorial forest of Gabon, Africa, where deep lateritic profiles have evolved by long-term weathering of the tectonically stable Congolese craton. Here, the transport-limited landscape enhances the formation of soils (Stallard, 1988). This weathering profile is representative of the global weathering system developed within the tropical forested belts in Africa and South America.

DONDO MOBI LATERITIC WEATHERING PROFILE

We chose a weathering system that, because of the distinct and well-characterized parent materials, offered ideal opportunities for deter-
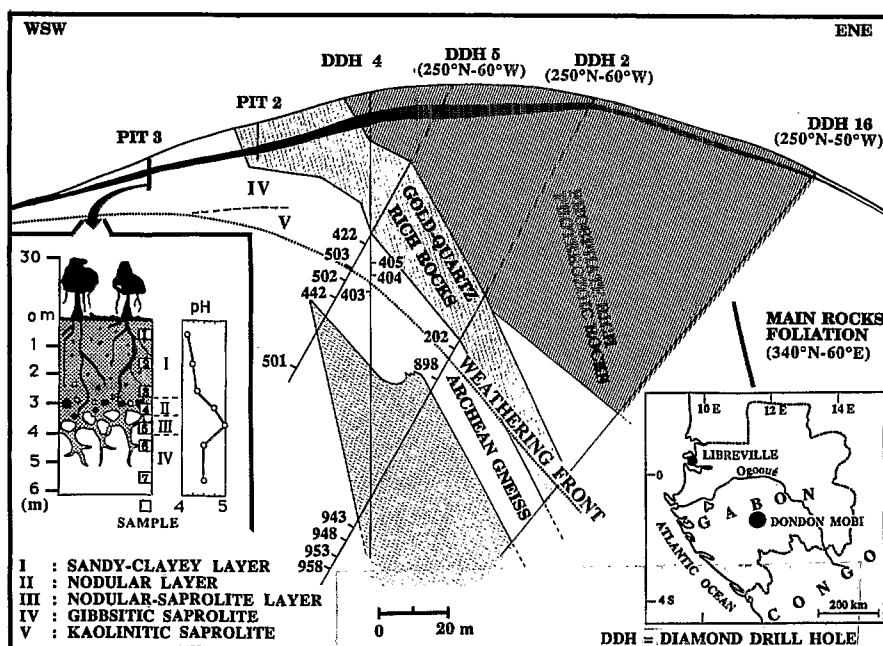

Figure 1. Dondo Mobi weathering profile: sandy-clayey layer (samples 1–3), nodular layer (sample 4), nodular-saprolite layer (sample 5), gibbsitic saprolite (samples 6 and 7), and kaolinitic saprolite (samples 422, 503, 405, 404, and 202).

mining weathering processes, and for separating open and closed chemical-system behavior.

The Dondo Mobi weathering mantle in the Eteke gold belt of southern Gabon developed on the Archean gneissic Congo craton at the expense of gneiss, gold- and quartz-rich hydrothermally altered komatiite, and Proterozoic phosphate-rich schist and quartzite (Colin and Vieillard, 1991) (Fig. 1). The weathering profile is differentiated into three main zones; from bottom to top these are the saprolite, nodular, and sandy clayey layers. Because the parent Archean gneisses are homogeneous, a requisite condition for the application of mass-balance models, we focus here on the weathering profile developed downslope, where an additional transitional nodular-saprolite layer has been found (Fig. 1).

X-ray diffraction and thin-section microscopy reveal that whereas quartz and muscovite are little weathered and quartz concentration is approximately constant, chlorite, feldspar, and biotite progressively disappear toward the nodular-saprolite layer and are replaced by goethite, kaolinite, and gibbsite. The two chemical and mineralogical saprolites distinguished are a kaolinite-rich saprolite located just above the weathering-front level, and a gibbsite-rich saprolite developed just above the 15 m surficial downslope weathering-front level. Both the nodular layer and the root-rich sandy-clayey layer consist of quartz and muscovite surrounded by a kaolinite-gibbsite-goethite-rich matrix. The underlying nodular-saprolite layer occurs between the saprolitic system and the upper layers. This differentiation points to four different weathering subsystems within the profile: (1) the kaolinitic saprolite, (2) the gibbsitic saprolite, (3) the nodular-saprolite layer, and (4) the nodular and the sandy clayey layers.

CHEMICAL AND PHYSICAL PROCESSES AS FUNCTIONS OF PORE CHARACTERISTICS

The relation between pores and mineralogical, textural, and structural properties of rocks in the four weathering subsystems was studied in oriented thin sections under petrographic microscope and oriented undisturbed bulk-rock samples under scanning electron microscope (SEM) with energy dispersive capability. The pore-size distribution was measured on two representative thin sections per sample by means of a computer-assisted digitizing petrographic system that gives an accurate modal count of pore volumes and sizes. In addition, grain density (ρ_g) and bulk density (ρ_w) were measured to calculate the bulk porosity:

$$\text{Porosity} = 1 - \frac{\rho_w}{\rho_g}. \qquad (1)$$

From the fresh rock to the surface, grain density varies little (Fig. 2A), and porosity depends linearly on bulk density, which decreases upward from 2.7 to 1.6 g/cm^3. Consequently, porosity increases from 0% in the fresh gneiss to 40% in its weathered surficial equivalent. Porosity increases in both the kaolinitic and gibbsitic saprolites, and remains con-

stant within the nodular and sandy-clayey layers above. These changes in porosity are explained by pore-size distribution (Fig. 2B) and pore type in relation to mineralogy (Fig. 3, A–H).

Two types of pores are found in the kaolinitic saprolite: sporadic mesopores (30–100 μm) and micropores (10–30 μm) visible only by SEM investigation. In Figure 3A, the mesopores are discontinuous but aligned following directions reflecting the physical weakness of the rocks, which are microfractures in the parent rock that resulted from microtectonic events. These paths are preferential avenues of meteoric water circulation, which promotes dissolution of the minerals. The micropores are intracrystallite pores that result from the textural organization of kaolinite crystals. Kaolinite ($\pm$goethite) pseudomorphically replaces chlorite, biotite, and feldspar (Fig. 3B). All chemical elements except aluminum are released to the ground water, though silicon and iron are partially retained.

In the gibbsitic saprolite, the porosity is characterized by a population of macropores (100–1000 μm) averaging 150 μm in diameter (Fig. 2B). These large pores are separated from each other by gibbsitic septa that mimic the intergranular and intragranular cleavage limits of primary minerals that are totally or partly dissolved (Fig. 3C). The gibbsitic matrix also invades large domains, obliterating the texture of the primary banded gneiss. In contrast to the kaolinitic matrix developed in the lower part of the profile, the gibbsitic matrix has no micropores, so most of the porosity of the rock is contributed by macropores (Fig. 3D).

The average pore size in the gibbsitic nodular-saprolite layer is 50 μm, and the maximum is 300 μm, much less than the maximum pore size of both underlying and overlying layers (Fig. 2B). All three pore-size classes are represented. This layer consists of abundant millimetre-sized gibbsitic domains similar to those observed in the underlying layer, crosscut by a yellow kaolinite-goethite-rich matrix (Fig. 3E). The texture of parent minerals is locally preserved in the gibbsitic zones, but the banded structure of the initial gneiss is lost. The pores within the gibbsitic matrix are partially filled with cutans composed of tiny kaolinite and goethite crystal assemblages (Fig. 3, E and F), which reduce pore sizes. These pores, however, are unconnected. At the top of the layer there are fine soil-root interface voids (Fig. 3E).

In the nodular and the sandy-clayey layers, the average pore size is ~100 μm; the maximum size increases from 600 μm in the nodular layer to 900–980 μm in the upper layer. The first of the two pore-size classes represented, micropores, is characterized by a homogeneous sandy-clayey matrix spreading throughout both layers (Fig. 3G). A few iron nodules are present in the nodular layer, which is crosscut by numerous vertical roots. The kaolinite-goethite-rich matrix exhibits vesicles totally infilled with components similar to the matrix, but often preserving curvature features. We conclude that this matrix resulted from physical and chemical evolution of the underlying layer under intense homogenizing bioturbation processes. The original gneiss texture is completely erased and replaced by a microaggregated pedogenic character, frequently described in equatorial
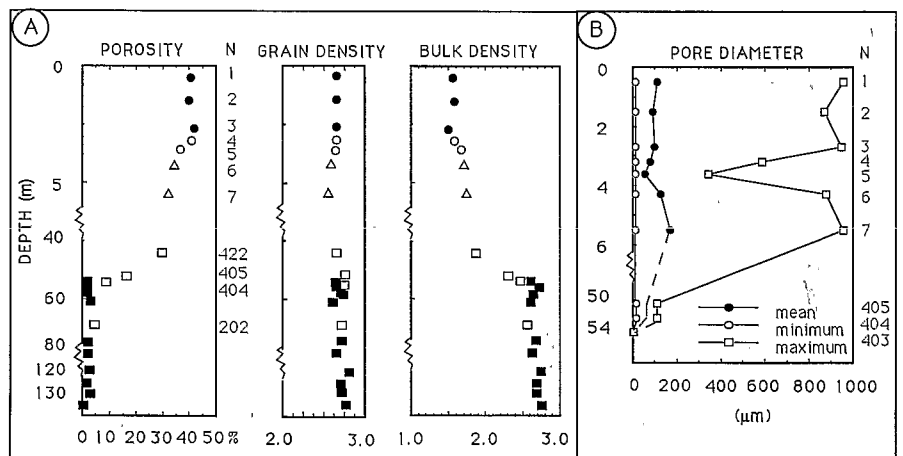

Figure 2. A: Variation in bulk porosity (%), grain density (g/cm^3), and bulk density (g/cm^3) with depth. Samples are identified by their respective number (**N**, related to Fig. 1) and by symbols for each weathering subsystem (solid circles = sandy-clayey and nodular layers, open circles = nodular, gibbsitic saprolite layer, open triangles = gibbsitic saprolite, open squares = kaolinitic saprolite) and for fresh rock (solid squares = unweathered gneiss). B: Distribution and size range of pores with depth.

soils. Only quartz and muscovite relicts, and gibbsitic pseudomorphs after feldspars, remain from the parent gneiss. A new generation of macropores is present as interaggregate pores or vertical, no longer active, root passages (Fig. 3, G and H). These pores are connected and have vesicular shapes. In such pores, numerous free heavy minerals such as zircons have been identified microscopically. As illustrated by the profile of the total heavy-mineral concentrations (Fig. 4A), this enrichment in heavy minerals is limited to the nodular and sandy-clayey layer. Because the maximum size of the heavy mineral (250 μm) is smaller than the maximum pore size of the nodular-saprolite layer (300 μm), we conclude that the downward translocation of heavy minerals within the lateritic profile is not limited by pore size, but instead by pore shape.

SOURCE OF TRANSLOCATED HEAVY MINERALS AND STRAIN EVOLUTION

The total weight percent of heavy minerals (0.025%) is constant from the fresh gneiss to the nodular-saprolite layer, but then increases upward to 0.26% of the total bulk sample (Fig. 4A). The increased proportion of heavy minerals can be explained either by closed-system processes such as residual enrichment of a collapsed system, or by open-system processes such as contamination with external material.

Digitizing petrographic microscope studies of heavy-mineral concentrates show that two populations of zircon are present: (1) perfectly euhedral, cloudy, and zoned grains ubiquitous in the profile, attributed to Archean gneiss, and (2) subrounded, cloudy grains present only in the nodular and sandy-clayey layers, similar in morphology to zircons related to gold-rich, hydrothermally altered rock and to Proterozoic sedimentary series recognized upslope (Fig. 1).

Because the euhedral zircons are residual from in situ weathering of the Archean gneiss and neither significant dissolution nor precipitation of zircon has been recognized, the corresponding zirconium concentration (C_{Zre}) can be used as an immobile index element in mass-balance equations. Volumetric changes (strain) can be calculated from equation 2 (Brimhall et al., 1988):

$$\epsilon_{Zr,w} = \frac{C_{Zr,p}}{C_{Zre,w}} \frac{\rho_p}{\rho_w} - 1, \tag{2}$$

where the subscripts p and w refer to parent and weathered rocks, respectively. The calculations (Fig. 4B) and petrological evidence reported above for each of the four weathering subsystems allow us to conclude that (1) the kaolinitic saprolites show no volumetric change and preserve the structure of the parent rock; (2) the gibbsitic saprolites are 26% to 33% collapsed with respect to the parent rock, an effect that can be attributed to strong dissolution and development of a massive gibbsitic matrix locally obliterating the parent texture; and (3) the gibbsitic nodular-saprolite layer is strongly collapsed (45%), corresponding petrographically to the loss of both texture and structure of the parent gneiss. This natural collapse does not reduce the total porosity of the rock, as in tillage-induced compaction (Glinsky and Lipiec, 1990) but, rather, reduces the pore size and modifies the pore type at constant overall porosity.

The nodular layer and the sandy-clayey layers are characterized by a progressive upward reexpansion (from –25% to 0%), which can be caused by root growth and burrowing animals.

To quantify the extraction or the addition of a chemical element (j) either by solute migration or mechanical translocation, we used the open-system mass-fraction transport function ($\tau_{j,w}$) (Brimhall et al., 1988):

$$\tau_{j,w} = \frac{\rho_w}{\rho_p} \frac{C_{j,w}}{C_{j,p}} (\epsilon_{Zr,w} + 1) - 1, \tag{3}$$

where the subscripts w and p refer to weathered rocks and parent rock, respectively. Because the calculation of $\tau_{j,w}$ takes into account both residual enrichment and deformation, a positive value for $\tau_{j,w}$ reflects a true mass gain in element j in the weathered rock compared to the parent rock, and a negative value indicates a mass loss.

FACTOR ANALYSIS AND INTERPRETATION

Relations between $\tau_{j,w}$ expressing chemical mass gains and losses with porosity and strain were established here by factor analysis for a data set consisting of 24 $\tau_{j,w}$ results and two physical properties (porosity and strain) calculated for 21 fresh and weathered samples.

Results show that 79% of the total variance in the data set is accounted for by two factors alone (Fig. 5). Factor 1 explains 42% of the variance in the weathering system and pertains to the behavior of rock-forming silicate minerals. Most of the elements (e.g., Si, Ca, Sr, Mg) in Figure 6A are simultaneously leached (negative $\tau_{j,w}$) out of the system during weathering as feldspar, biotite, and chlorite alter to kaolinite or gibbsite. In contrast to these leached elements, $\tau_{j,w}$ is zero or positive and results essentially from residual enrichment and minor introduction. The
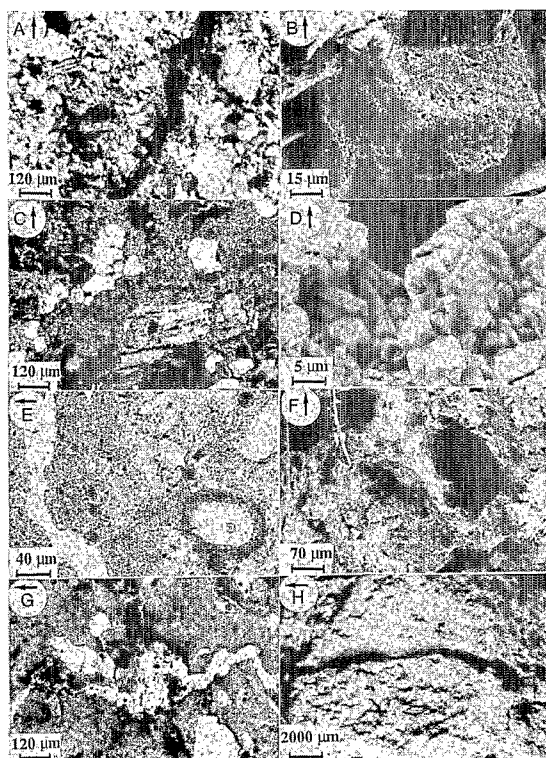
Figure 3. Micromorphological features of weathered rocks under polarizing microscope (A, C, E, G), under scanning electron microscope (B, D, F), and under binocular microscope (H). Arrows indicate upward vertical orientation. See text for details.
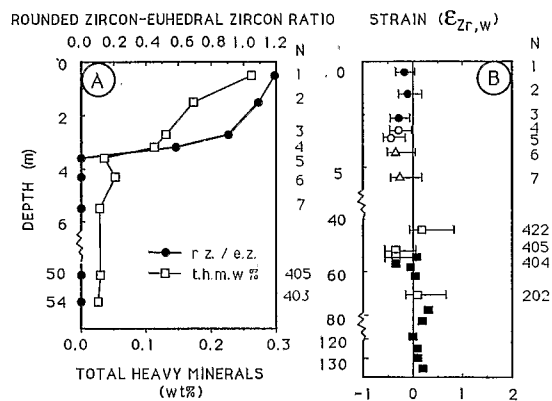
Figure 4. A: Variation in total heavy-mineral weight percent (t.h.m.w.%) and rounded zircon/euhedral zircon ratio (r.z./e.z.) with depth. B: Variation in strain (on basis of immobile behavior of zirconium accounted for by euhedral zircons) with depth. Error bars have been calculated from maximum and minimum protore zirconium contents. Samples are identified by their respective numbers (N, related to Fig. 1).

Figure 5. Results of factor analysis carried out on chemical (τ) and physical data obtained for entire set of rock and soil samples. Both τ and strain have been calculated using immobile zirconium concentrations corresponding to euhedral zircon (A). In factor score representation (B), dashed arrow shows weathering path.
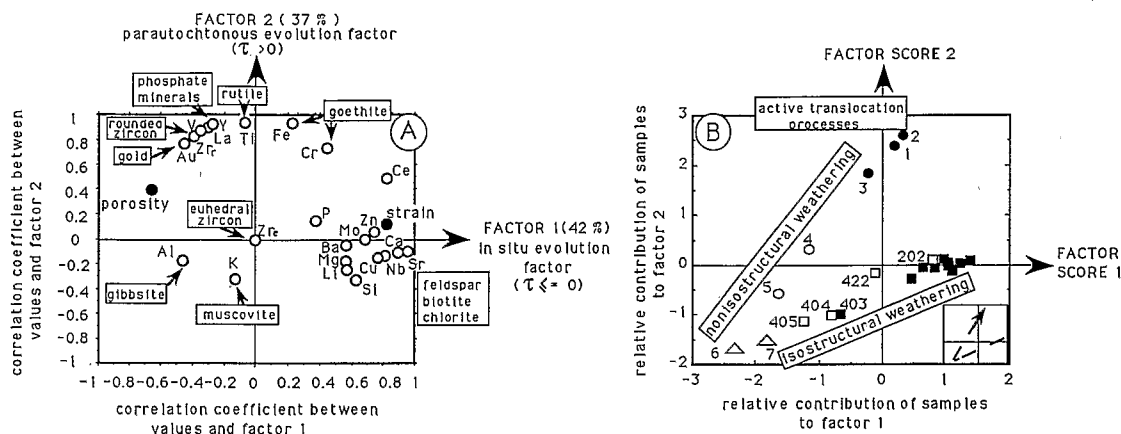
partial retention of K is attributed to the resistance of muscovite to weathering. A negative strain (collapse) is strongly positively correlated to the leaching of mobile elements (negative $\tau_{j,w}$), inducing pore development. Factor 1 thus quantifies the in situ dissolutional evolution of the lateritic profile and its residual enrichment.

Factor 2 explains 37% of the total variance and pertains to chemically stable accessory minerals (Fig. 5A). All the elements for which the $\tau_{j,w}$ results are positive (e.g., Ti, Au, Fe) are strongly positively correlated and are introduced into the upper nodular and sandy-clayey layers through connected macropores. These elements implicate heavy minerals already described as the rounded zircons (Zr_r and mobile minerals such as rutile and phosphate minerals identified by SEM as micrometric xenotime, monazite, and gorceixite, as well as gold particles. Because rutile and phosphate minerals, present as residual components of the weathering profile developed upslope from the Proterozoic rocks and gold particles, are detrital phases derived from gold-rich rocks (Colin and Vieillard, 1991) (Fig. 1), we conclude that these minerals are physically moved from nearby sources and do not involve chemical solute transport and reprecipitation.

Factor 2, therefore, quantifies the parautochthonous evolution of the open weathering system that develops by superimposition onto the in situ evolution in the upper part of the profile. Petrological examination (Fig. 3) and mass-balance calculations (Fig. 5, A and B) show that no mechanical translocations of upslope quartz (a main component of upslope rocks) occur in the downslope Archean gneiss profile, precluding intensive downslope creep or larger scale erosion. We postulate, therefore, that the translocation of heavy minerals through macropores results from progressive selective processes during weathering mantle development.

In Figure 5B, the weathering pathway is shown sample by sample. It demonstrates an evolution from the fresh rock to the soils along progressive stages of in situ isostructural weathering essentially controlled by dissolution processes, followed by a superimposed path of deformation in the upper layers, within which translocation processes dominate upward.

CONCLUSIONS

Rock, meteoric water, and biological agents interact in equatorial forests to develop open biochemical lateritic weathering systems, which undergo chemical and physical evolution expressed in the dynamic evolution of pores, mineral assemblages, deformation, and mass transfer of elements. Within such an ecosystem, the subsystems behave as porous compartments forming a geomembrane filter. In addition to the effects of biochemical cycling, which accumulates carbon and nitrogen components in soils (Kempe, 1988), the geomembrane filtration effect causes a distinct spatial fractionation of minerals and chemical elements through each compartment. With respect to the parent rock, some elements remain in the lateritic soils (Al in K from muscovite and Zr_e), some are imported from nearby sources (Au, Ti, La, Zr_r, Fe, V, and Cr), and others leave the soil profile in ground-water discharge (Si, Li, Sr, Mg, Ca, Ba, and K from

feldspar). From the surface to the fresh rock, the imported elements, heavy minerals, suspended particles, and solutes are gradually filtered. In the sandy-clayey and nodular layer, intense bioturbation and pedoturbation (Eschenbrenner, 1988) promote the transfers of heavy minerals, suspended particles, and solutes. In the underlying nodular-saprolite layer, only suspended matter and solute can be imported, whereas dissolved elements are selectively filtered in the saprolitic system.

The mechanical selectivity of a given compartment depends upon structural and chemical properties of the filter. Limiting factors in translocation are the state of natural deformation, the mineral identity, and the shapes and sizes of pores rather than the net porosity. Roots play an essential role in providing connected pathways for mineral translocation and maintenance of high porosity during conversion from deeper isostructural weathering to bioturbated material.

REFERENCES CITED

Anamosa, P.R., Nkedi-Kizza, P., Blue, W.G., and Sartain, J.B., 1990, Water movement through an aggregated, gravelly oxisol from Cameroon: Geoderma, v. 46, p. 263–281.
Arnold, R.W., Szabolcs, I., and Targulian, V.O., eds., 1990, The report of an IIASA-ISSS-UNEP task force on the role of soils in global change: Laxenburg, Austria, International Institution of Applied System Analysis, 110 p.
Brimhall, G.H., Lewis, C.J., Ague, J.J., Dietrich, W.E., Hampel, J., Teague, T., and Rix, P., 1988, Metal enrichment in bauxites by deposition of chemically mature eolian dust: Nature, v. 333, p. 819–824.
Colin, F., and Vieillard, P., 1991, Behavior of gold in the lateritic equatorial environment: Weathering and surface dispersion of residual gold particles, at Dondo Mobi, Gabon: Applied Geochemistry, v. 6, p. 279–290.
Eschenbrenner, V., 1988, Les glébules des sols de Côte d'Ivoire: Paris, Institut Français de Recherche Scientifique pour le Développement et la Coopération (ORSTOM), Mémoire 498 p.
Glinsky, J., and Lipiec, J., 1990, Soil physical conditions and plant roots: Boca Raton, Florida, CRC Press, 250 p.
Kempe, S., 1988, Freshwater carbon and the weathering cycle, in Lerman, A., and Meybeck, M., eds., Physical and chemical weathering in geochemical cycles: Dordrecht, Netherlands, Kluwer, p. 197–223.
Lacroix, A., 1914, Les latérites de la Guinée et les produits d'altération qui leur sont associés: Nouvelles Archives Muséum, v. 5, p. 255–356.
Lean, J., and Warrilow, D.A., 1989, Simulation of the regional climatic impact of Amazon deforestation: Nature, v. 342, p. 411–413.
Millot, G., 1964, Géologie des argiles: Paris, Masson et Cie, 499 p.
Nahon, D.B., 1991, Introduction to the petrology of soils and chemical weathering: New York, John Wiley & Sons, 313 p.
Stallard, R.F., 1988, Weathering and erosion in the humid tropics, in Lerman, A., and Meybeck, M., eds., Physical and chemical weathering in geochemical cycles: Dordrecht, Netherlands, Kluwer, p. 225–246.
Sternberg, H.O., 1987, Aggravation of floods in the Amazon River as a consequence of deforestation?: Geografiska Annaler, v. 69A, p. 201–219.